2011-06

Optimal Control of the Unsteady Euler Equations in 1D with Application to Ignition Overpressure Attenuation in Launch Vehicles

20th AIAA Computational Fluid Dynamics Conference
27 - 30 June 2011, Honolulu, Hawaii

AIAA 2011-3847

Optimal Control of the Unsteady Euler Equations in 1D with Application to Ignition Overpressure Attenuation in Launch Vehicles

Nathan D. Moshman * and Garth V. Hobson †
Naval Postgraduate School, Monterey, CA, 93943, USA
Sivaguru S. Sritharan ‡
Naval Postgraduate School, Monterey, CA, 93943, USA

This paper presents a new formulation and computational solution of an optimal control problem concerning unsteady shock wave attenuation. The adjoint system of equations for the unsteady Euler system in 1D is derived and utilized in an adjoint-based solution procedure for the optimal control. A novel algorithm is used to solve for the optimal control solution that satisfies all necessary first order optimality conditions while locally minimizing an appropriate cost functional. The solution procedure is sufficiently flexible such that it can be used to solve other distributed optimal control problems where the state dynamics are in the form of non-linear hyperbolic systems of partial differential equations and where the initial data is given and the final data is free at a free final time. Distributed control solutions with certain physical constraints are calculated for attenuating blast waves similar to to those generated by Ignition Over Pressure (IOP) from the Shuttle's Solid Rocket Booster during launch. The control solutions give insight to the magnitude and location of energy dissipation necessary to decrease a given blast wave's overpressure to a set target level over a given spatial domain while using only as much control as needed.

Nomenclature

J	Cost Functional
a, b	Weighting Constants
T	Final Time
Ω	Spatial Domain in 1D
$\partial\Omega$	Spatial Domain Boundary
z	Control Variable
P	Gas Pressure
Q	Target Pressure at Final Time
h	Final Time Penalty
U	3-Component State Vector
ρ	Gas Density
ρu	Gas Momentum
u	Gas Velocity
ρE	Gas Total Energy
ρe	Gas Internal Energy
γ	Gas Constant
L	Running Cost Functional (Lagrangian)
H	Hamiltonian

*PhD Candidate, Mechanical and Aerospace Engineering Departmant, 700 Dyer Road Monterey, CA 93943, AIAA Student Member
†Professor, Mechanical and Aerospace Engineering Departmant, Mail Code: MAE/Hg Monterey, CA 93943, AIAA Member
‡Research Professor, Office of the Dean of Research, 1 University Circle Monterey, CA 93943

V 3-Component Adjoint Vector
A Jacobian Matrix
$\tilde{J}$ Augmented Cost Functional
ϵ positive small constant
f Functional of Final Time
m_{H_20} Energy Equivalent Vaporized Water Mass
L_{hv} Latent Heat of Vaporization of Water at 100° C
OP_0 Absolute Pressure just behind shock front of uncontrolled IOP blast wave
x 1D spatial vector in Ω
Subscript
i, j, k Variable number
Superscript
n Control algorithm iteration number
$*$ Optimal quantity

I. Introduction

Ignition over pressure (IOP) is a phenomenon present at the start of an ignition sequence in launch vehicles using solid grain propellants. When the grain is ignited the pressure inside the combustion chamber quickly rises several orders of magnitude. This drives hot combustion products toward the nozzle and out to the open atmosphere at supersonic speeds. An IOP wave is a spherical blast wave which originates from the exit plane of the nozzle and propagates spherically outward near Mach 1. Over pressures that the body of the rocket experiences are of the order 2:1.[1] The region just outside the nozzle will experience further compression due to displacement of gas along the blast wave's direction of propagation and over pressures can approach 10:1. The portions of the IOP wave that become incident on the rocket body or launch platform components must have an over pressure below a known threshold to avoid costly damage. The current technique used by NASA and other launch providers is to spray water into the region around the nozzle before ignition. This forces the IOP wave to propagate through water before becoming incident on the rocket body or platform components. Through *several* dissipative mechanisms this causes a sufficient decrease to the pressure jump across the shock as to prevent damage. The implementation of the water suppression system is ad-hoc, specific to the shuttle, and has not been reconsidered in decades. The latest work from NASA was a parametric study of water arrangement in the nozzle region and how it affected the maximum IOP strength.[2,3] Cannabal's dissertation is the first work on parametrically optimizing IOP attenuation with respect to water injection strategy. The goal of this work is to develop a computational tool that can directly calculate a distributed optimal control for attenuating a range of blast waves to a desired minimal overpressure.

II. Computational Fluid Dynamics

Data on the shuttle grain and chamber pressure[4] was input to Cequel[5] a code for steady state rocket property calculations. The output gives the temperature and gas velocity at the nozzle exit plane for a given pressure ratio. Initially, ambient conditions inside the domain are present. The ignition sequence was simulated in 2D using the ESI-Fastran Solver.[6] Constant mass-flow boundary conditions equivalent to the steady state exit plane of the rocket nozzle on the shuttle were used in the bottom center of the domain on the right face of the step as shown in Figure 1. Pressure is depicted in three snapshots in Figures 1.a, 1.c and 1.e and Mach number in Figures 1.b, 1.d, and 1.f. The last frame is roughly 10 ms after ignition. The bottom left edge of the domain represents the rocket body while the bottom right edge is the centerline of the normal to the nozzle exit plane and a symmetry boundary. All other edges are non-reflecting boundaries.

Flow conditions over time were recorded at two locations marked in Figure 1.a. Point 1 is near the rocket body 2.5 meters above the nozzle and Point 2 is 1.5 meters along the symmetry boundary and the plane normal to the nozzle exit. The conditions at the recorded locations are used as the boundary conditions in the 1D Euler Equations calculation used for the optimal control calculation. Figure 2.a shows the flow conditions over time at Monitor Point 1 near the rocket body and Figure 2.b shows the flow conditions over time for Monitor Point 2 directly downstream of the nozzle.

The single phase control calculation is meant to give insight into a multiphase control calculation where

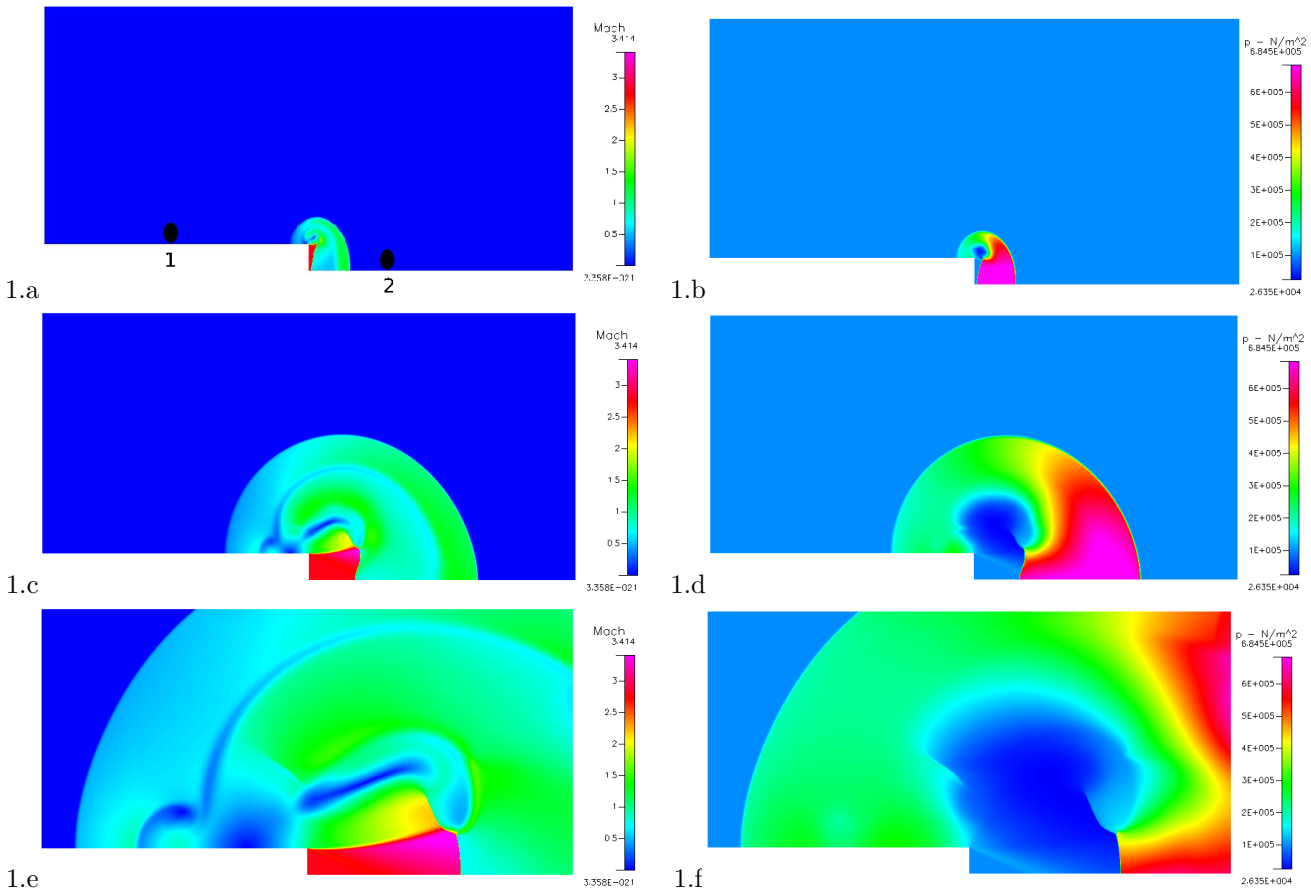

Figure 1: Simulated Shuttle IOP: Mach Number at (1.2ms, 4ms, 10ms) after ignition (1.a, 1.c, 1.e); Pressure at (1.2ms, 4ms, 10ms) after ignition (1.b, 1.d, 1.f)

water placement determines shock attenuation. A multiphase fluid system has 2(3N)+1 independent state variables where N is the number of spatial dimensions. Conservation of mass, momentum and energy are obeyed for both the gas and the liquid and the final equation conserves the volume fraction of each phase. Therefore the 1D multiphase calculation is a seven state system. Several interaction mechanisms between the water droplets and the IOP wave are present and not fully understood. The dominant dissipative mechanism for shocks between Mach 1 and 2 is the loss of energy of the gas through vaporization of the water droplets.[7] Experimental data from droplet-shock interaction in this regime shows that the other dissipative mechanisms e.g. drag on droplets, sensible heating of droplets etc. are less significant to IOP attenuation. In a multiphase calculation, the control action would take the form of a liquid mass source and the effect of vaporization will take energy out of the gas phase. To most simply replicate the dominant dissipative mechanism with a single phase calculation, the control will act as an energy sink with no corresponding mass or momentum sinks or sources.

A conservative Godunov-type method, second order accurate in space, proposed by Tadmor[8] and Van Leer,[9] was implemented to solve the compressible flow dynamics in 1D under a distributed control action. This method assumes that the solution in each cell is piece-wise linear and projects an intermediate solution on a non-uniform grid based on the maximum characteristic speeds from the interpolated solutions at each cell interface. The familiar Godunov integration on the uniform grid is then second order accurate because of the intermediate finer grid. This numeric method can be adapted to the solution of a 1D multiphase calculation as presented in Saurel and Abgrall.[10]

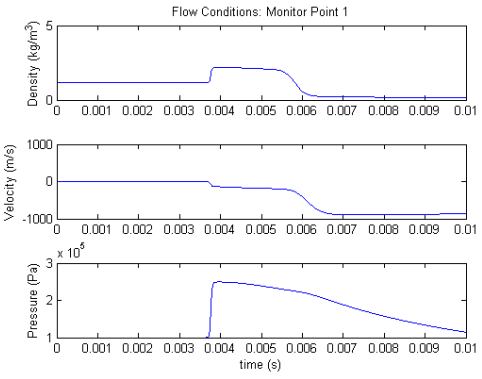

2.a

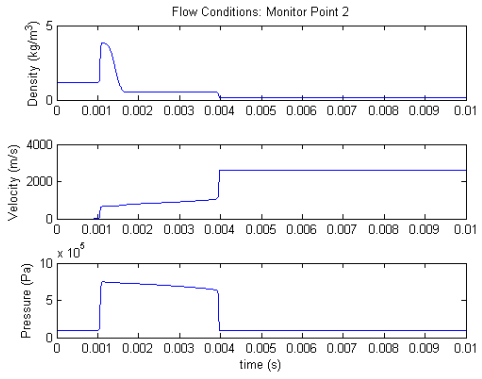

2.b

Figure 2: Flow conditions over time for Points 1 and 2

III. The Optimal Control System

In any optimal control problem there is a cost functional to minimize. In this context it must reflect that a decrease in the maximum jump in pressure (the overpressure at the shock front) is most desirable. It should also penalize control action but to a lesser magnitude. Therefore let J be the cost functional.

$$J = \frac{a}{2}\int_0^T \int_\Omega z(x,t)^2 dx dt + \frac{b}{2}\int_\Omega (P(x,T) - Q(x))^2 dx \tag{1}$$

Here x represents a spatial vector, one dimensional in this calculation. T is the final time which is not fixed, $z(x,t)$ is the control action, $P(x,T)$ is the Pressure at the final time, $Q(x)$ is the desired final pressure and a and b are weighting constants. The larger b is compared to a, the more significant the final time penalty and the less the penalty for using control action. The final time penalty will be denoted as h for convenience.

$$h(U(x,T)) = \frac{b}{2}\int_\Omega (P(x,T) - Q(x))^2 dx \tag{2}$$

The control action will take the form of an internal energy sink. It only appears on the right hand side of the energy balance equation of the 1D Euler system.

$$U = (\rho(x,t), \rho u(x,t), \rho E(x,t))^T \tag{3}$$

$$\frac{\partial}{\partial t}\begin{pmatrix} \rho \\ \rho u \\ \rho E \end{pmatrix} + \frac{\partial}{\partial x}\begin{pmatrix} \rho u \\ \rho u^2 + P \\ u\,(\rho E + P) \end{pmatrix} = \begin{pmatrix} 0 \\ 0 \\ z(x,t) \end{pmatrix} \tag{4}$$

$$\rho E = \rho e + \frac{\rho u^2}{2} \tag{5}$$

$$P = \rho e\,(\gamma - 1) \tag{6}$$

Initial conditions are stationary, ambient air. Stating the density, velocity and pressure determines the internal and total energy and the conservative vector.

$$\begin{aligned} \rho(x,0) &= 1\ kg/m^3 \\ u(x,0) &= 0\ m/s \\ P(x,0) &= 10^5\ Pa \\ \rho u(x,0) &= 0\ kg \cdot m/s \\ \rho e(x,0) &= 250000\ J \\ \rho E(x,0) &= 250000\ J \end{aligned} \tag{7}$$

The inlet boundary condition is explicitly given by the IOP simulation data shown in Figures 2.a and 2.b when the flow is supersonic. If the flow is subsonic, non-reflection of the $u - c$ characteristic is imposed.[12] In addition, the Monitor Point data was chosen where the flow was nearest to 1D; however, the 2D data did have transverse motion. The data will still give a plausible 1D blast wave with the inlet boundary condition set in this manner and the goal of the calculation, controlling a range of blast waves, can be achieved. At the outlet boundary the flow remains stationary because the final time will always be such that the shock wave will not have enough time to propagate though the entire domain and reach the outlet.

In order to determine the optimal control $z^*(x,t)$ that minimizes the cost functional J it is necessary to define the Hamiltonian of the system and derive necessary conditions using the Pontryagin Minimum Principle and the calculus of variations. The Hamiltonian for this system is:

$$\begin{aligned} H(U,V,z,t) &= L(U,z) + \int_\Omega V \cdot \frac{\partial U}{\partial t} dx \\ &= \int_\Omega \frac{a}{2} z^2 + V_1 \frac{\partial \rho}{\partial t} + V_2 \frac{\partial (\rho u)}{\partial t} + V_3 \frac{\partial (\rho E)}{\partial t} dx \end{aligned} \tag{8}$$

(V_1, V_2, V_3) is the co-state or adjoint vector. Writing the Euler equations in non-conservative form in this basis defines the Jacobian matrix.

$$\frac{\partial U_i}{\partial t} + A_{ij}(U) \frac{\partial U_j}{\partial x} = z_i \delta_{i3} \tag{9}$$

$$A_{ij}(U) = \begin{pmatrix} 0 & 1 & 0 \\ \frac{(\rho u)^2}{\rho^2} \frac{\gamma - 3}{2} & -\frac{(\rho u)}{\rho} (\gamma - 3) & (\gamma - 1) \\ \frac{-\gamma (\rho u)(\rho E)}{\rho^2} + (\gamma - 1) \frac{(\rho u)^3}{\rho^3} & \frac{\gamma (\rho E)}{\rho} - \frac{3}{2} (\gamma - 1) \frac{(\rho u)^2}{\rho^2} & \frac{\gamma (\rho u)}{\rho} \end{pmatrix} \tag{10}$$

To derive necessary conditions the optimal state must be defined $(U^*(x,t), P^*(x,t), z^*(x,t), T^*)$ and the optimal control perturbed such that $z = z^* + \epsilon \delta z$ where $\epsilon > 0$ is a small constant. The variation in the control will cause variational terms in each of the other free variables of the system that must necessarily vanish at an optimal solution. To incorporate the constraints of the 1D Euler system using the Lagrange multiplier method, multiply each conservation law by an adjoint variable and add this term to J. This is the augmented cost functional $\tilde{J}$. Then from expanding $\tilde{J}$ in a Taylor series the first order necessary condition will be:

$$\frac{d}{d\epsilon} \tilde{J} (z^* + \epsilon \delta z) \,|_{\epsilon = 0} = 0 \tag{11}$$

Grouping the terms of like variational multipliers gives the optimal system. Integrating by parts until all derivatives are on the adjoint vector yields the following linear system of partial differential equations.[11]

$$\frac{\partial V_j}{\partial t} + A_{ij}\frac{\partial V_i}{\partial x} + \left(\frac{\partial A_{ij}}{\partial x} - \frac{dA_{ij}}{dU_k}\cdot\frac{\partial U_k}{\partial x}\right)V_i + \frac{\partial}{\partial x}\left[\left(A_{ij}v_i^*, \delta u_j\right)\right]|_{\partial\Omega} = \frac{\partial L}{\partial U_i} = 0 \tag{12}$$

Non-trivial elements of the matrix $\frac{dA_{ij}}{dU_k}\cdot\frac{\partial U_k}{\partial x}$ are given in Appendix A. $\partial\Omega$ denotes the boundary of the spatial domain. The right hand side of Equation (12) is zero in this formulation because the running cost does not explicitly depend on the state vector.

Since the final state is not fixed there is a necessary condition on the adjoint vector at the final time.

$$V_i^*\left(x, T^*\right) = \frac{\partial}{\partial U_i}h\left(U\left(x, T^*\right)\right) \tag{13}$$

Therefore, in *this* basis, all 3 derivatives are non-zero.

$$\begin{aligned}
V_1^*\left(x, T^*\right) &= b\left(P\left(x, T^*\right) - Q(x)\right)\frac{\partial P}{\partial \rho}\left(x, T^*\right) \\
&= b\left(P\left(x, T^*\right) - Q(x)\right)\frac{u\left(x, T^*\right)^2}{2}\left(\gamma - 1\right) \\
\\
V_2^*\left(x, T^*\right) &= b\left(P\left(x, T^*\right) - Q(x)\right)\frac{\partial P}{\partial\left(\rho u\right)}\left(x, T^*\right) \\
&= -b\left(P\left(x, T^*\right) - Q(x)\right)u\left(x, T^*\right)\left(\gamma - 1\right) \\
\\
V_3^*\left(x, T^*\right) &= b\left(P\left(x, T^*\right) - Q(x)\right)\frac{\partial P}{\partial\left(\rho E\right)}\left(x, T^*\right) \\
&= b\left(P\left(x, T^*\right) - Q(x)\right)\left(\gamma - 1\right)
\end{aligned} \tag{14}$$

For a free final time the necessary condition for the optimal final time T^* is given by the Transversality condition. f is a funtional to be used in the solution procedure.

$$\begin{aligned}
H\left(U^*\left(x, T^*\right), V^*\left(x, T^*\right), z^*\left(x, T^*\right), T^*\right) + \frac{d}{dt}h\left(U\left(x, T^*\right)\right) &= 0 \\
\\
\int_\Omega \frac{a}{2}z(x, T^*)^2 + b(P(x, T^*) - Q(x))\begin{pmatrix} \frac{\partial P}{\partial \rho}\left(x, T^*\right)\frac{\partial \rho}{\partial t}\left(x, T^*\right) + \\ \frac{\partial P}{\partial \rho u}\left(x, T^*\right)\frac{\partial \rho u}{\partial t}\left(x, T^*\right) + \\ \frac{\partial P}{\partial \rho E}\left(x, T^*\right)\frac{\partial \rho E}{\partial t}\left(x, T^*\right) + \\ \frac{\partial P}{\partial t}\left(x, T^*\right)\end{pmatrix} dx &= 0 \\
\\
&\equiv f(T^*)
\end{aligned} \tag{15}$$

The necessary condition on the optimal control solution comes from maximizing the Hamiltonian for an unconstrained control. The unconstrained condition is justified because there is no restriction on control magnitude in regions where control is allowed. The integral is true over any domain Ω and at any moment in time it should be true point-wise for all $t \in [0, T]$.

$$\frac{\partial H}{\partial z}\left(U^*, V^*, z^*, t\right) = \int_{\Omega} a z^*(x,t) + V_3^*(x,t) dx = 0 \tag{16}$$

Equations (3)-(7),(12),(14),(15) and (16) give the complete set of first order necessary conditions for the optimal system.

IV. Solution Procedure

Define the left hand side of the Transversality Condition in Equation (15) as a continuous function $f(T)$ with independent variable as the final time. Then $f(T^*) = 0$. T^* can be solved iteratively with the Newton-Raphson root finding method.

$$T^{n+1} = T^n - \frac{f\left(T^n\right)}{\frac{df}{dt}\left(T^n\right)} \tag{17}$$

$$\begin{aligned} \lim_{n\to\infty} T^{n+1} &= T^* \\ \lim_{n\to\infty} f\left(T^{n+1}\right) &= f\left(T^*\right) = 0 \end{aligned} \tag{18}$$

The overall algorithm which is used to satisfy all of the above necessary optimal conditions is shown in block-diagram form in Figure 3.

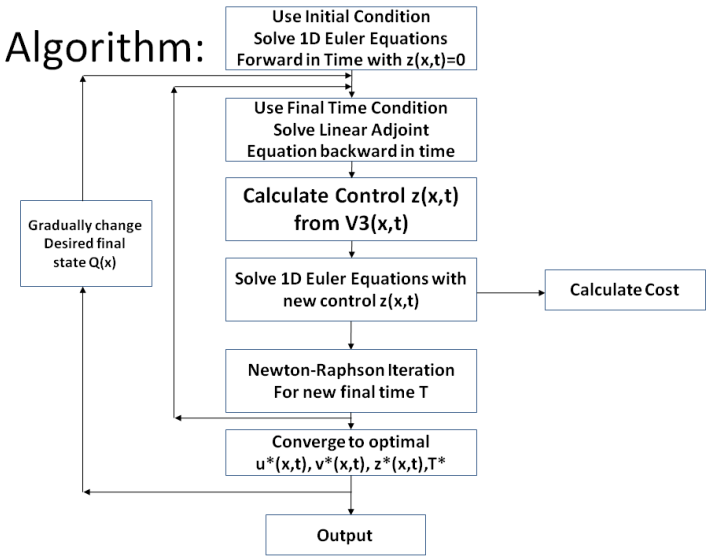

Figure 3: Block Diamgram of Solution Procedure

V. Results and Discussion

The solution procedure in Figure 3 assumes a given target state $Q(x)$ at the final time T^*. To illustrate trends in the optimal control solution, prescribing a consistent and meaningful target state or sequence of target states is a necessity. The target state prescribed for the first example, shown in the plots of Figure 4 has 85% of the amplitude of the final pressure profile when no control is used OP_0. This attenuated pressure profile replaces the uncontrolled pressure profile from just behind the shock front to 30 cm from the inlet boundary. The target is then linearly increased to the magnitude of the uncontrolled pressure profile over 10cm. Upstream of the shock, the target state is such that only pressures greater than the target pressure are penalized. The nonlinear nature of shock waves means that not all target states may be possible for the given initial conditions and boundary conditions. In addition, the purpose of the calculation is to calculate control solutions which decrease overpressure and therefore the cost functional should not penalize pressures below the target pressure. Furthermore, error near the shock front is not directly penalized but is still minimized via the iterative update to the final time from Equation (16). In each of the given examples the weighting constants a and b are 10^{-6} and 10^4 respectively. Since b is much larger than a, minimizing J is dominated by minimizing h. The value for b is such that the magnitude of the third adjoint variable $V_3(x,t)$, and thus the control action $z(x,t)$ are sufficient to cause noticeable attenuation to the blast wave.

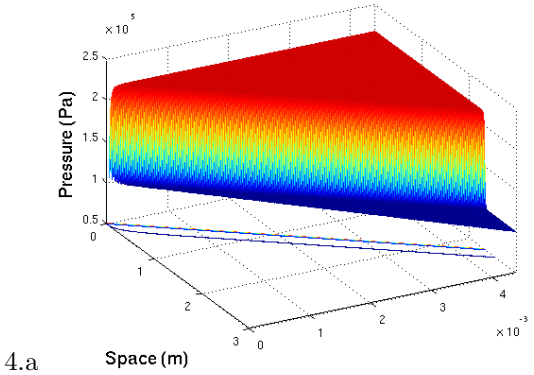

4.a

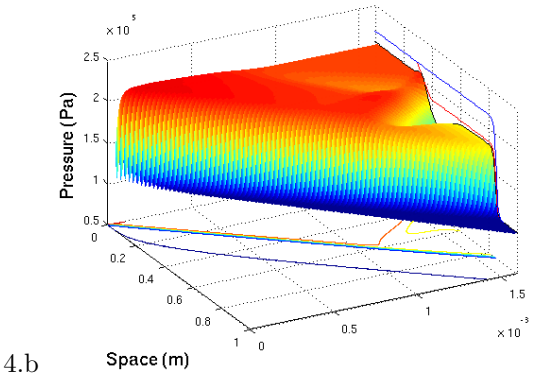

4.b

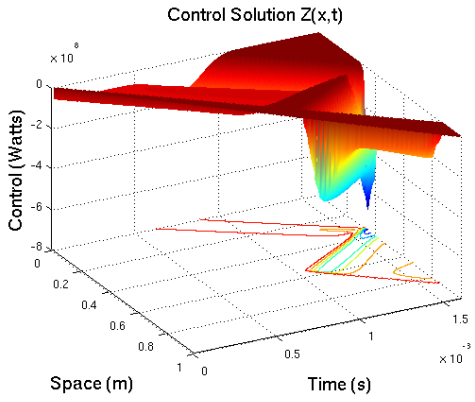

4.c

Figure 4: Monitor Point 1, Target State Penalizes Pressure above 85% of uncontrolled OP: (4.a) $P(x,t)$ with $z(x,t) = 0$, (4.b) $P^*(x,t)$ in $1m$ domain, (4.c) $z^*(x,t)$ in $1m$ domain

The surface plots in Figures 4-7 represent converged results of the optimization algorithm. Figure 4.a is a surface plot of the pressure from the data at Monitor Point 1 in Figure 2.a over a 3 meter domain with no control used. Figure 4.b shows the pressure when under the calculated optimal control action. The uncontrolled pressure profile at the final time is shown in blue and the target state is shown in red. Figure 4.c. is the distributed optimal control solution. Both Figure 4.b and 4.c are in a 1 meter domain. Figures 4.d and 4.e are in a 2 meter domain and Figures 4.f and 4.g are in a 3 meter domain. The larger domain

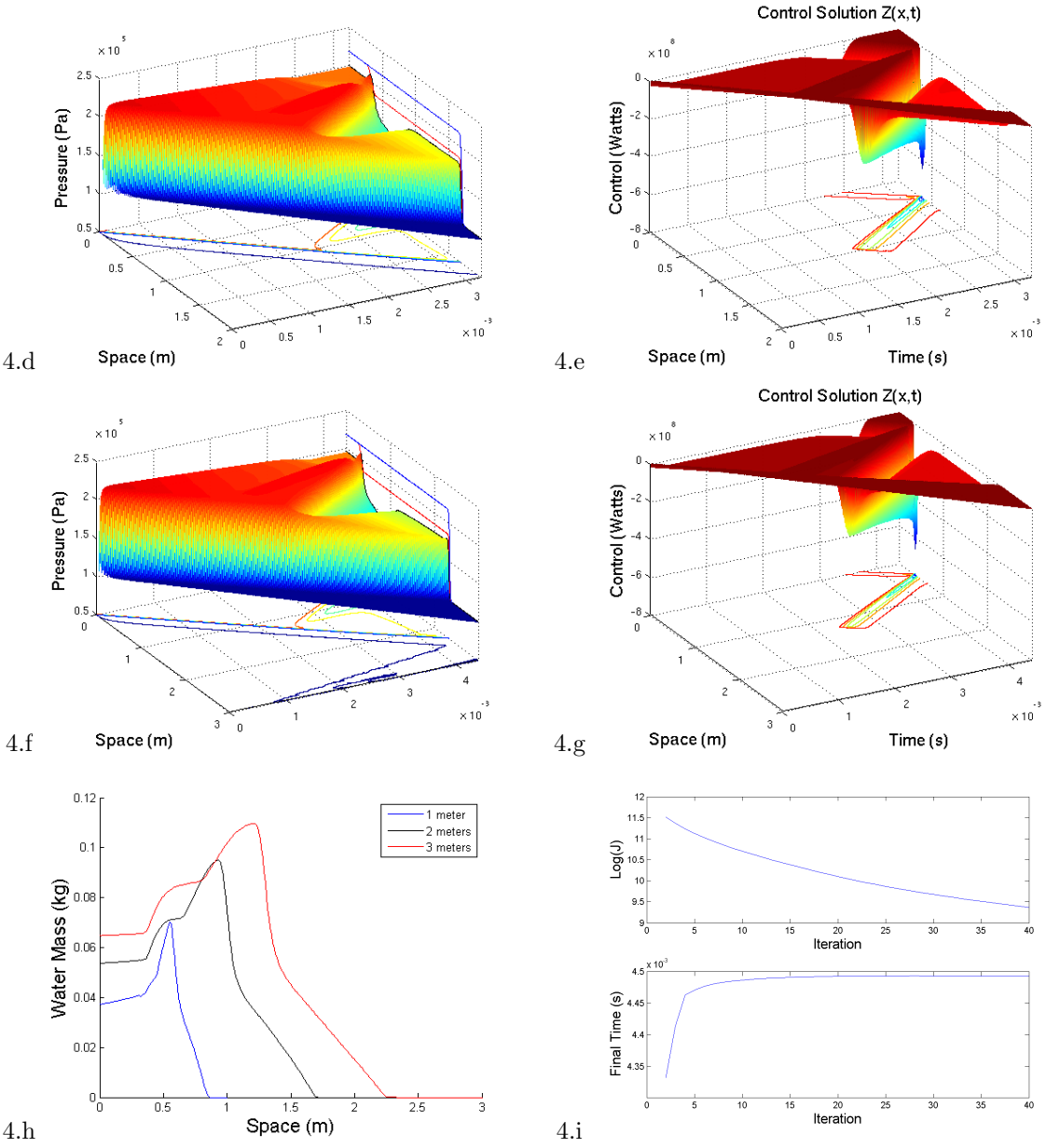

4.d 4.e 4.f 4.g 4.h 4.i

Figure 4: Monitor Point 1, Target State Penalizes Pressure above 85% of uncontrolled OP: (4.d) $P^*(x,t)$ in $2m$ domain, (4.e) $z^*(x,t)$ in $2m$ domain, (4.f) $P^*(x,t)$ in $3m$ domain, (4.g) $z^*(x,t)$ in $3m$ domain,(4.h) $m_{H_20v}(x)$ Energy equivalent of vaporized water mass (4.i top) Log of Cost Functional J over iterations of solution procedure (4.i bottom) Optimal Final Time T^* over iterations of solution procedure

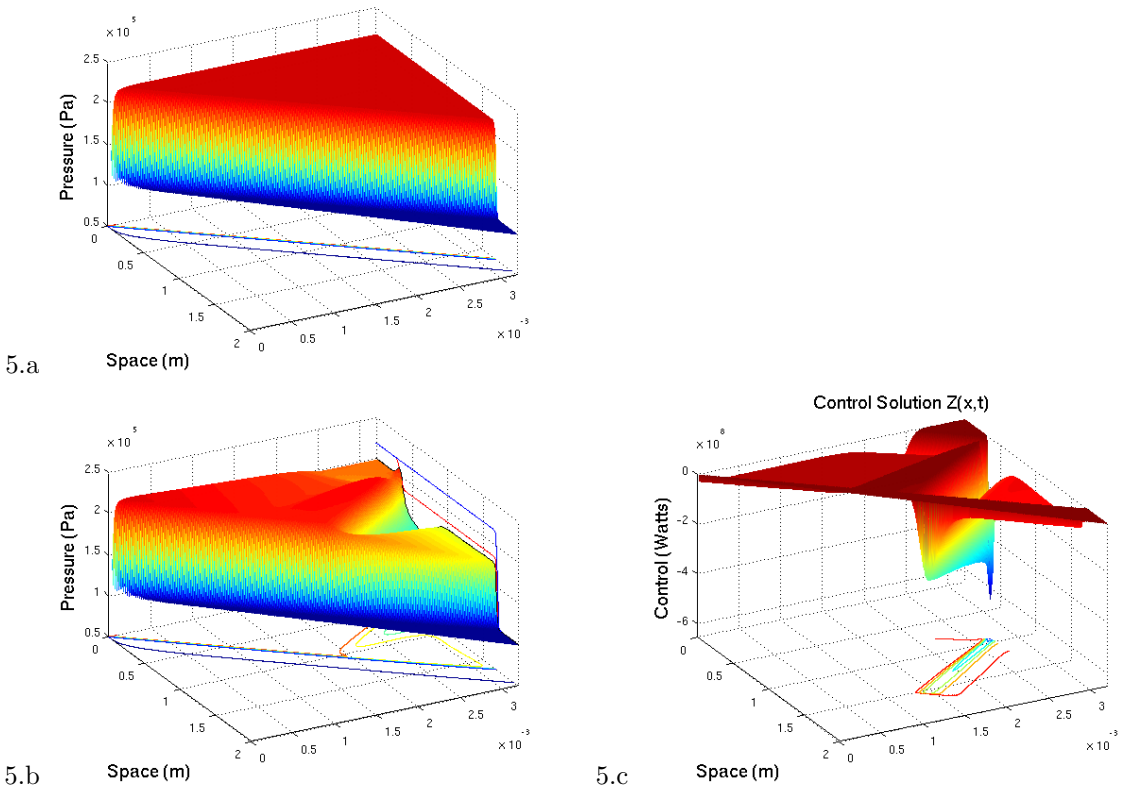

5.a

5.b

5.c

Figure 5: Monitor Point 1, Target State Penalizes Pressure above 85%, 80% and 75% of uncontrolled OP in a 2 meter domain: (5.a) $P(x,t)$ with $z(x,t) = 0$, (5.b) $P^*(x,t)$ for 85% OP_0, (5.c) $z^*(x,t)$ for 85% OP_0

means that the same overpressure attenuation level is required over a larger length.

In each example a physical restriction on the control is imposed such that energy can only be taken out of the gas *behind* the shock wave. This more accurately portrays how discrete droplet sprays will sink energy from the gas via vaporization. The plots shown in Figures 4.h are distributions of the energy equivalent vaporized water mass to the optimal control solutions. By dimensional analysis, inspection of the energy balance equation indicates that the units of $z^*(x,t)$ are Watts. Integrating the control solution from $[0, T^*]$ gives an energy distribution in space. This energy can be directly equated to an amount of water mass that must be vaporized using the latent heat of vaporization of waterL_{hv} = -2.26e6 J/kg at 100° C. Equation (19) precisely relates the optimal control solution, distributed in space and time, to an equivalent distribution of water mass vaporized over the same time interval.

$$m_{H_20v}(x) = \frac{1}{L_{hv}} \int_0^{T^*} z^*(x,t)dt \tag{19}$$

Figure 4.h shows how that affects the equivalent water distribution based on Equation (19). Water takes time to vaporize and therefore cannot sink energy from the gas instantaneously and arbitrarily close to the shock front. In practice, water will take energy out of the gas at least a meter behind the shock front. That less energetic gas will then drive the shock with less energy and the pressure profile will flatten out to a diminished overpressure. With more detailed physically-based restrictions on the control action, this single phase shock wave control formulation can be made to better replicate a two-phase shock-droplet interaction control calculation without the considerable added complexity of a two-phase compressible flow model. Regardless, trends in the data seem heuristically correct and therefore empirical scaling laws in magnitude and location may be sufficient.

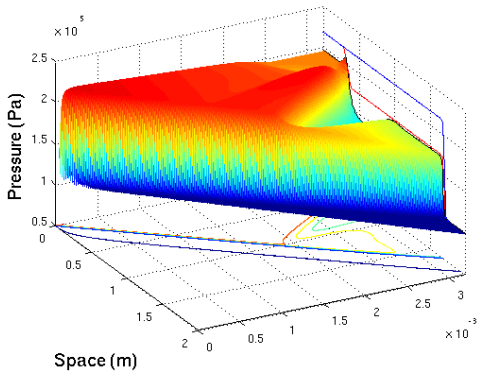

5.d

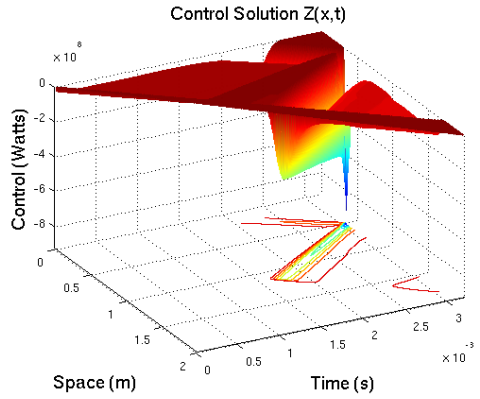

5.e

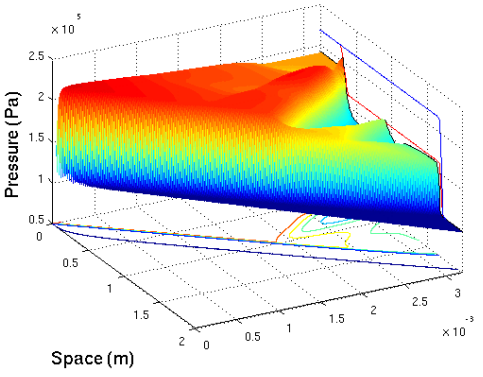

5.f

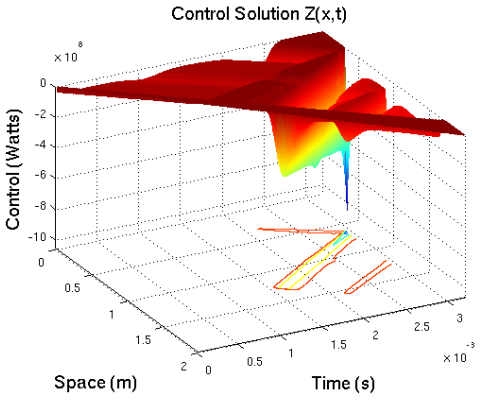

5.g

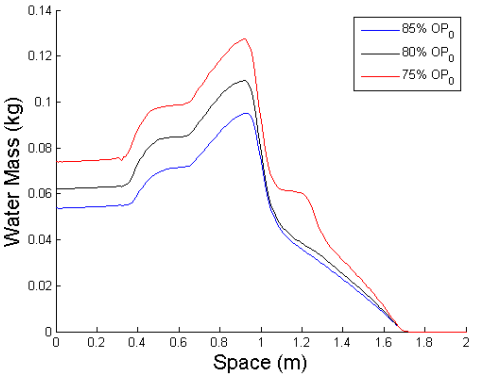

5.h

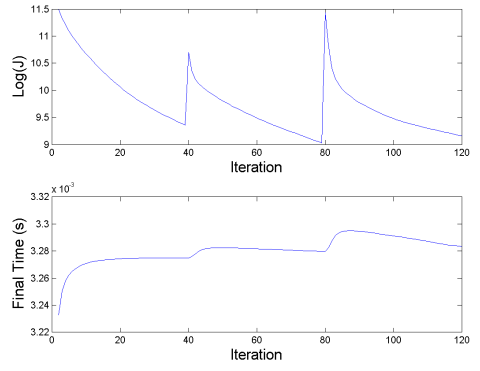

5.i

Figure 5: Monitor Point 1, Target State Penalizes Pressure above 85%, 80% and 75% of uncontrolled OP in a 2 meter domain: (5.d) $P^*(x,t)$ for 80% OP_0, (5.e) $z^*(x,t)$ for 80% OP_0, (5.f) $P^*(x,t)$ for 75% OP_0, (5.g) $z^*(x,t)$ for 75% OP_0, (5.h) $m_{H_20v}(x)$ Energy equivalent of vaporized water mass (5.i top) Log of Cost Functional J over iterations of solution procedure (5.i bottom) Optimal Final Time T^* over iterations of solution procedure

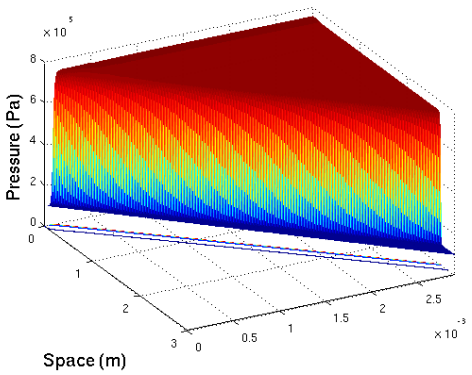

6.a

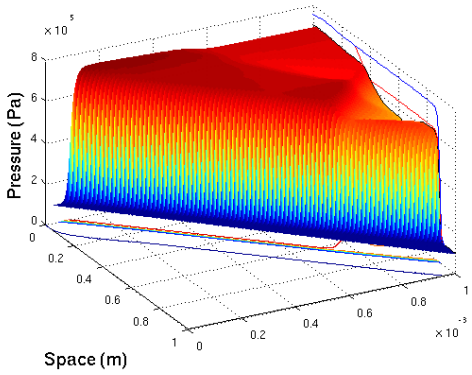

6.b

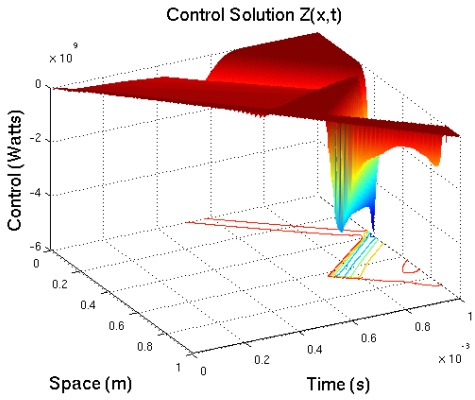

6.c

Figure 6: Monitor Point 2, Target State Penalizes Pressure above 85% of uncontrolled OP: (6.a) $P(x,t)$ with $z(x,t) = 0$, (6.b) $P^*(x,t)$ in $1m$ domain, (6.c) $z^*(x,t)$ in $1m$ domain

The top plot in Figure 4.i shows the logarithm of the cost functional J over the solution iterations for the 3 meter case. The bottom plot in Figure 4.i shows the corresponding final time solution iterates with $T^0 = 4$ ms. A negative control in the energy equation can be thought of as an internal energy sink. Temperature is directly related to internal energy, so the control action cools the gas. A cooler gas has a lower speed of sound. Consequently it will take longer for the shock front in the wave interacting with control to reach the same point in space that the shock without control reached. Additionally, from a hyperbolic wave theory point-of-view, a non-linear wave travels slower if it has less amplitude. The control action's purpose is to attenuate amplitude and this necessarily slows the wave down. The Transversality Condition is very sensitive to error at the shock front since this is where the time rate of change of the pressure is greatest. It would be a difficult matter to get significant attenuation in a converged solution with a fixed final time for this reason.

Figure 5.a is a surface plot of the pressure from the data at Monitor Point 1 over a 2 meter domain with no control used. Figure 5.b shows the pressure when under the calculated optimal control action. The uncontrolled pressure profile at the final time is shown in blue and the target state is shown in red. In this example, the target state is in a fixed domain of 2 meters and the level of overpressure attenuation is increased. Figure 5.b is the optimal pressure solution with a target state that has 85% of the uncontrolled overpressure. Figure 5.c. is the corresponding distributed optimal control solution. Figures 5.d and 5.e are the optimal pressure and control solutions respectively for a target state that has 80% of the uncontrolled overpressure. Figures 5.f and 5.g are the optimal pressure and control solutions respectively for a target state that has 75% of the uncontrolled overpressure. Figure 5.h shows how the energy equivalent vaporized water mass increases for decreasing target over pressures. The top plot in Figure 5.i is the logarithm of the cost functional J over solution iterations. The additional feature of changing the target state during the solution procedure is demonstrated in this example. The jumps in J at the 40th and 80th iteration indicate that the target state $Q(x)$ has been redefined with a lower overpressure. The bottom plot in Figure 5.i again shows that the optimal final time T^* increases with increasing overpressure attenuation. Here, $T^0 = 3.2$ ms.

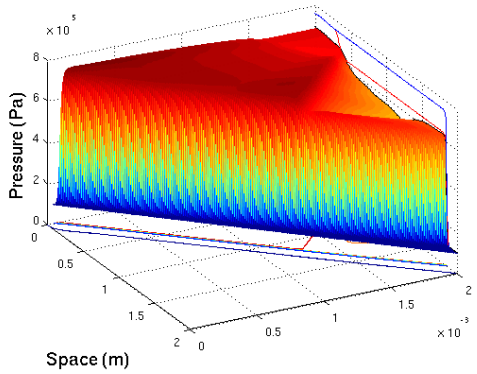

6.d

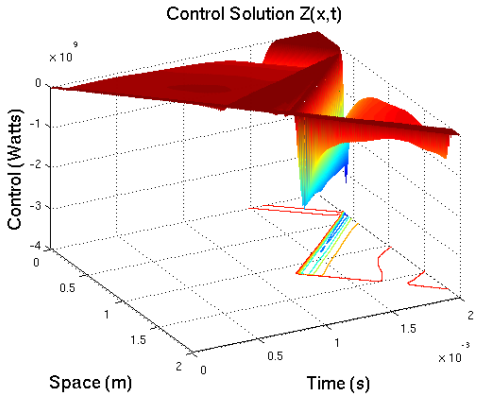

6.e

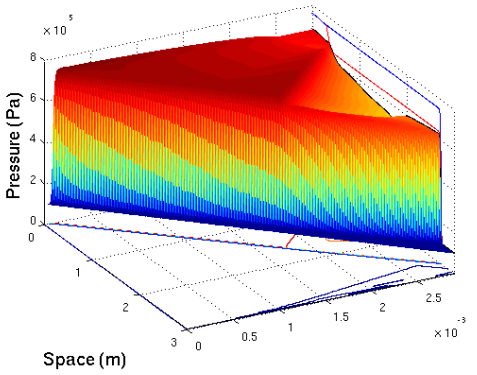

6.f

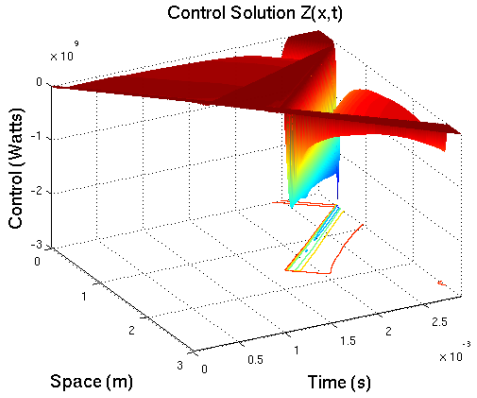

6.g

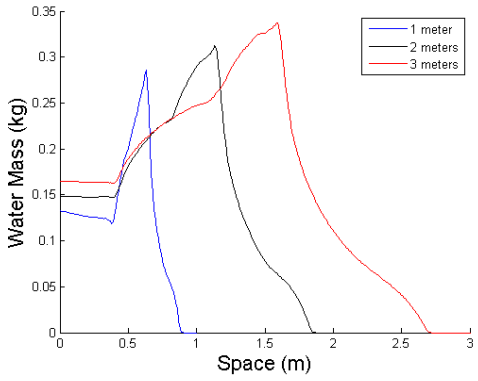

6.h

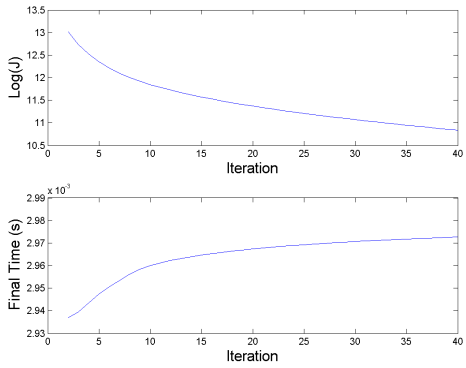

6.i

Figure 6: Monitor Point 2, Target State Penalizes Pressure above 85% of uncontrolled OP: (6.d) $P^*(x,t)$ in $2m$ domain, (6.e) $z^*(x,t)$ in $2m$ domain, (6.f) $P^*(x,t)$ in $3m$ domain, (6.g) $z^*(x,t)$ in $3m$ domain,(6.h) $m_{H_20v}(x)$ Energy equivalent of vaporized water mass (6.i top) Log of Cost Functional J over iterations of solution procedure (6.i bottom) Optimal Final Time T^* over iterations of solution procedure

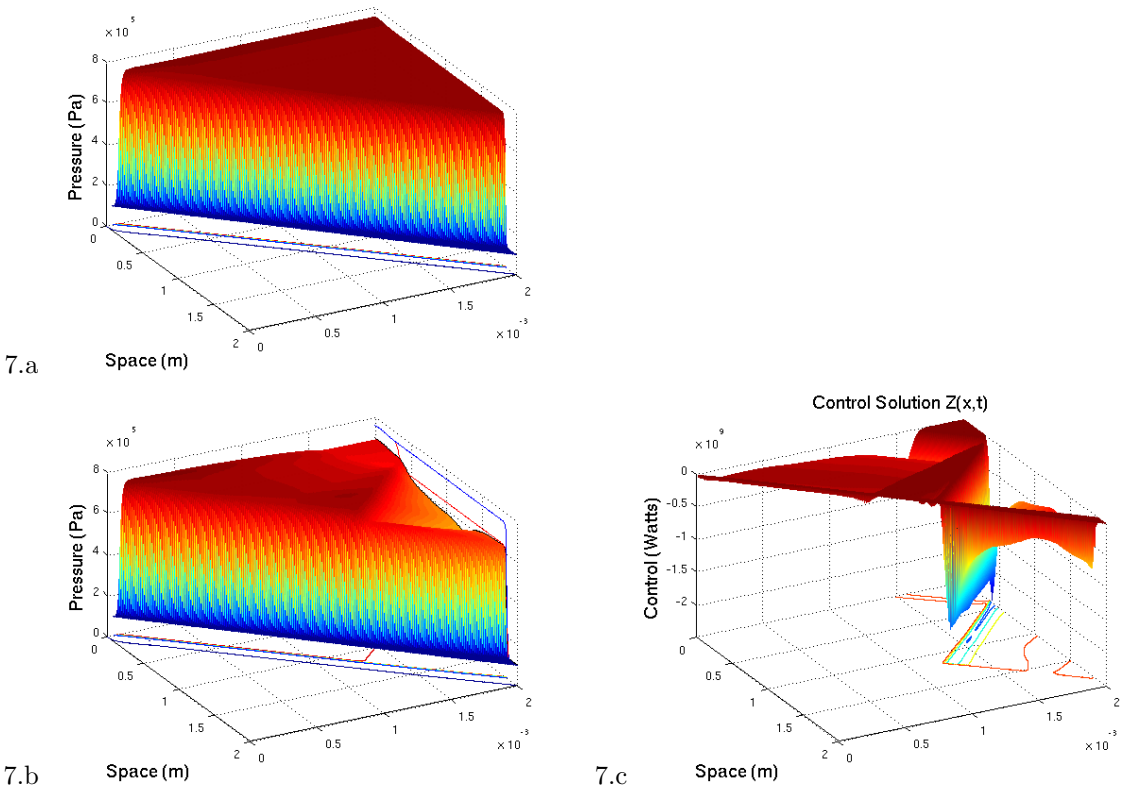

7.a 7.b 7.c

Figure 7: Monitor Point 2, Target State Penalizes Pressure above 85%, 70% and 50% of uncontrolled OP in a 2 meter domain: (7.a) $P(x,t)$ with $z(x,t) = 0$, (7.b) $P^*(x,t)$ for 85% OP_0, (7.c) $z^*(x,t)$ for 85% OP_0

The third example, shown in the plots of Figure 6, uses the blast wave data from Monitor Point 2 shown in Figure 2.b along the symmetry line in the shuttle blast wave simulations. As in the first example, the target states are pressure profiles with 85% of the uncontrolled overpressure in a 1 meter, 2 meter and 3 meter domain. This blast wave has a much larger overpressure, 8:1, and the gas is much hotter. Hotter gas has more ability to vaporize water and here vaporization may be most effective toward shock attenuation. The experimental data mentioned earlier was not relevant for blast waves with over pressures this large and recent results indicate that kinetic sinks-large amounts of water-may be necessary for protecting the bottom of the launch pad from the IOP blast induced below the nozzle. Indeed video coverage of the water injection system during a shuttle launch attests to the immense amount of water used for mitigating IOP induced damage to the launch pad.

Figure 6.a is the pressure profile of the uncontrolled blast wave using the simulation data from Monitor Point 2 in 3 meter domain. Figure 6.b is the optimal pressure solution interacting with the optimal control solution shown in Figure 6.c in a 1 meter domain. Figure 6.d is the optimal pressure solution interacting with the optimal control solution shown in Figure 6.e in a 2 meter domain. Figure 6.e is the optimal pressure solution interacting with the optimal control solution shown in Figure 6.f in a 3 meter domain. Figure 6.g shows the energy equivalent vaporized water mass for a constant level of attenuation in increasing domain size. The top plot of Figure 6.i shows the value of the cost functional over the solution iterates for the 3 meter case. The bottom plot of Figure 6.i shows the corresponding solution iterates for the final time with $T^0 = 2.9$ ms.

Figure 7.a is a surface plot of the pressure from the data at Monitor Point 2 over a 2 meter domain with no control used. Figure 7.b shows the pressure when under the calculated optimal control action. The uncontrolled pressure profile at the final time is shown in blue and the target state is shown in red. In this example, the target state is in a fixed domain of 2 meters and the level of overpressure attenuation is

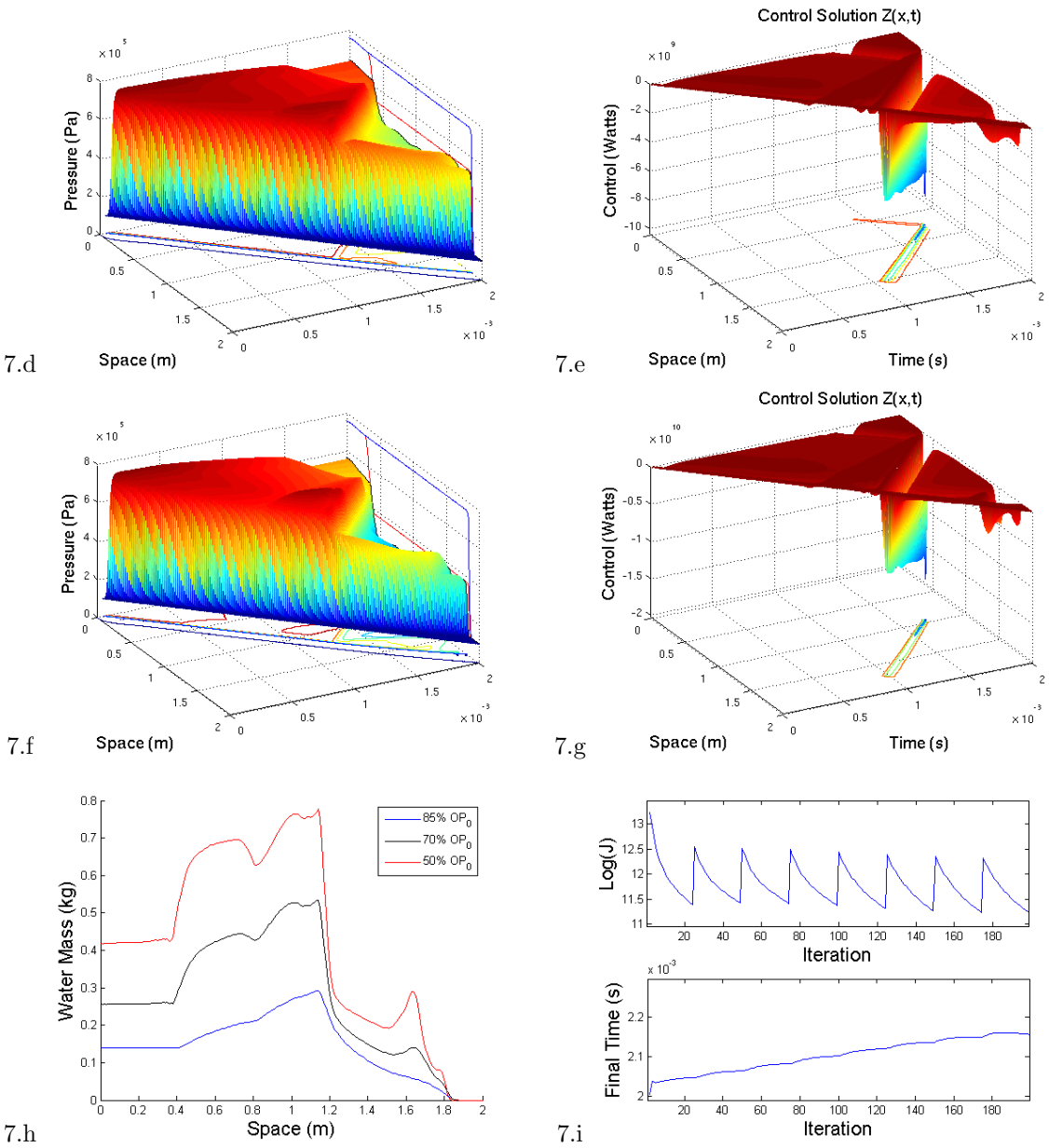

Figure 7: Monitor Point 2, Target State Penalizes Pressure above 85%, 70% and 50% of uncontrolled OP in a 2 meter domain: (7.d) $P^*(x,t)$ for 70% OP_0, (7.e) $z^*(x,t)$ for 70% OP_0, (7.f) $P^*(x,t)$ for 50% OP_0, (7.g) $z^*(x,t)$ for 50% OP_0, (7.h) $m_{H_2 0v}(x)$ Energy equivalent of vaporized water mass (7.i top) Log of Cost Functional J over iterations of solution procedure (7.i bottom) Optimal Final Time T^* over iterations of solution procedure

increased. Figure 7.b is the optimal pressure solution with a target state that has 85% of the uncontrolled overpressure. Figure 7.c. is the corresponding distributed optimal control solution. Figures 7.d and 7.e are the optimal pressure and control solutions respectively for a target state that has 70% of the uncontrolled overpressure. Figures 7.f and 7.g are the optimal pressure and control solutions respectively for a target state that has 50% of the uncontrolled overpressure. Figure 7.h shows how the energy equivalent vaporized water mass increases for decreasing target over pressures. The top plot in Figure 7.i is the logarithm of the cost functional J over solution iterations. The jumps in J every 25th iteration indicate that the target state $Q(x)$ has been redefined with a lower overpressure. The bottom plot in Figure 5.i shows the corresponding final time T^* iterates with $T^0 = 2$ ms.

The desired state cannot be directly set as described but must be gradually scaled down to the desired overpressure to assure convergence of the algorithm. It was found that when starting with an overpressure of 8:1, setting a target state with 85% of the uncontrolled overpressure, as in Figures 4 and 6, was about the most attenuation to the shock that could be desired and still maintain convergence of the the algorithm. The reason for this can be understood in the nature of the optimal system. The optimal conditions are all coupled and inter-dependent such that a calculated blast wave under no control action is in no way close to the optimal pressure profile of a blast wave under considerable damping control action so as to render a blast wave with a significantly diminished overpressure. When the final time solution is not nearly optimal, then first-order corrections to these terms are not enough to exploit in an iterative sense toward finding an optimal control satisfying all necessary conditions.

Another strategy to setting the desired pressure profile could involve prescribing a wave with a more gradual rise in pressure near the shock front, essentially smearing out the shock. The final time penalty would then involve the spatial derivative, and perhaps the temporal derivative, of the pressure rather than the magnitude of overpressure at the shock front.

VI. Conclusion

A new iterative solution procedure was developed which can calculate optimal distributed control solutions for systems of quasi-linear hyperbolic partial differential equations with free final data and final time. This procedure has been successfully applied to single-phase, one-dimensional compressible gas dynamics with the goal of diminishing overpressure at the shock front. Examples of optimal attenuation to blast waves typically encountered in the launch environment of the Shuttle's SRBs during an ignition are given. For a characterized dissipative mechanism (e.g. water droplets) the generated control solutions will give insight as to the magnitude and spatial distribution of energy equivalent vaporized water mass required to achieve a given level of overpressure reduction.

Appendix A: Non-zero elements of $\frac{d}{du_k} A_{ij} \frac{\partial u_k}{\partial x}$:

$$\frac{d}{du_k} A_{21} \cdot \frac{\partial u_k}{\partial x} = (\gamma - 3) \left(-\frac{u^2}{\rho} \frac{\partial \rho}{\partial x} + \frac{u}{\rho} \frac{\partial (\rho u)}{\partial x} \right) \tag{20}$$

$$\frac{d}{du_k} A_{22} \cdot \frac{\partial u_k}{\partial x} = (\gamma - 3) \left(\frac{u}{\rho} \frac{\partial \rho}{\partial x} - \frac{1}{\rho} \frac{\partial (\rho u)}{\partial x} \right) \tag{21}$$

$$\frac{d}{du_k} A_{31} \cdot \frac{\partial u_k}{\partial x} = \frac{u}{\rho} \left(2\gamma E - 3(\gamma - 1) u^2 \right) \frac{\partial \rho}{\partial x} + \frac{1}{\rho} \left(3(\gamma - 1) u^2 - \gamma E \right) \frac{\partial (\rho u)}{\partial x} - \gamma \frac{u}{\rho} \frac{\partial (\rho E)}{\partial x} \tag{22}$$

$$\frac{d}{du_k} A_{32} \cdot \frac{\partial u_k}{\partial x} = \frac{1}{\rho} \left(3(\gamma - 1) u^2 - \gamma E \right) \frac{\partial \rho}{\partial x} - 3(\gamma - 1) \frac{u}{\rho} \frac{\partial (\rho u)}{\partial x} + \frac{\gamma}{\rho} \frac{\partial (\rho E)}{\partial x} \tag{23}$$

$$\frac{d}{du_k} A_{33} \cdot \frac{\partial u_k}{\partial x} = -\frac{\gamma u}{\rho} \frac{\partial \rho}{\partial x} + \frac{\gamma}{\rho} \frac{\partial (\rho u)}{\partial x} \tag{24}$$

Acknowledgments

N. D. Moshman would like to thank Professors Chris Brophy, Frank Giraldo and Wei Kang at the Naval Postgraduate School and Bruce Vu at NASA Kennedy Space Center. In addition, N. D. Moshman thanks the Naval Postgraduate School and the Army Research Office for funding this research.

References

[1]Walsh, E., J., and Hart, P., M., "Flight-Measured Lift-off Ignition Overpressure- A Correlation with Subscale Model Tests," Martin Marietta Aerospace, *AIAA-81-2458*, Las Vegas, N.V., November 11-13, 1981.

[2]Canabal, F., III., "Suppression of the Ignition Overpressure Generated by Launch Vehicles," Ph.D. Dissertation, Mechanical and Aerospace Engineering Department, University of Alabama, Huntsville, AL., 2004.

[3]Jourdan, G., Biamino, L., Mariani, C., Blanchot, C., Daniel, E., Massoni, J., Houas, L., Tosello, R., and Praguine, D., "Attenuation of a Shock Wave Passing Through a Cloud of Water Droplets" *Shock Waves,* published online April 29, 2010; Vol. 20, Number 4, 2010 pp. 285-296.

[4]Sutton, G. and Biblarz, O., "Solid Propellant Rocket Fundamentals," *Rocket Propulsion Elements* 8th ed., John Wiley and Sons. Hoboken, New Jersey, 2010, pp. 437-438.

[5]Software Engineering Associates, Inc. Cequel Chemical Equilibrium in Excel, Available http://cearun.grc.nasa.gov/

[6]ESI group. CFD-FASTRAN-Manual, Available from http://www.esigroup.com/

[7]Schwer, D., and Kailasanath, K., "Blast Mitigation by Water Mist 2, Shock Wave Mitigation using Glass Particles and Water Dropltes," NRL/MR/6410–03-8658, January 21, 2003.

[8]Kurganov, A., and Tadmor, E., "New High-Resolution Central Schemes for Nonlinear Conservation Laws and Convection-Diffusion Equations," *Journal of Computational Physics,*published online December 8, 1999; Vol. 160, 2000, pp. 241-282.

[9]Van Leer, B., "Toward the Ultimate Conservative Difference Scheme. V. A Second-Order Sequel to Godunov's Method," *Journal of Computational Physics,* published July 1979 Vol. 32, pp. 101-136.

[10]Saurel, R., and Abgrall, R., "A Multiphase Godunov Method for Compressible Multi-fluid and Multiphase Flows," *Journal of Computational Physics,* published online Dec. 14, 1998; Vol. 150, 1999, pp. 425-467.

[11]Bressan, A., and Marson, A., "A Maximum Principle for Optimally Controlled Systems of Conservations Laws," *Rendiconti del Seminario Matematico della Universita di Padova,* tome 94, 1995, pp. 79-94.

[12]Merkle, C.,L., "Computational Fluid Dynamics of Inviscid and High Reynolds Number Flows," Unpublished Notes.